Nonperturbative photon $q\bar{q}$ light front wave functions from a contact interaction model

Chao Shi,[1,*] Zhongtian Yang,[1] Xurong Chen,[2] Wenbao Jia,[1] Cuibai Luo,[3,†] and Wenchang Xiang[4,‡]

[1]*Department of Nuclear Science and Technology, Nanjing University of Aeronautics and Astronautics, Nanjing 210016, China*

[2]*Institute of Modern Physics, Chinese Academy of Sciences, Lanzhou 730000, China*

[3]*Department of Physics, Anhui Normal University, Anhui 241002, China*

[4]*Physics Division, Guangzhou Maritime University, Guangzhou 510725, China*

(Received 1 November 2023; accepted 24 January 2024; published 21 February 2024)

We propose a method to calculate the $q\bar{q}$ light front wave functions (LFWFs) of photons at low virtuality, i.e., the light front amplitude of $\gamma^* \to q\bar{q}$ at low Q^2, based on a light front projection approach. We exemplify this method using a contact interaction model within Dyson-Schwinger equations formalism and obtain the nonperturbative photon $q\bar{q}$ LFWFs. In this case, we find the nonperturbative effects are encoded in the enhanced quark mass and a dressing function of covariant quark-photon vertex, as compared to the leading order quantum electrodynamics photon $q\bar{q}$ LFWFs. We then use nonperturbative-effect modified photon $q\bar{q}$ LFWFs to study the inclusive deep inelastic scattering HERA data in the framework of the color dipole model. The results demonstrate that the theoretical description of data at low Q^2 can be significantly improved once the nonperturbative corrections are included in the photon LFWFs.

DOI: 10.1103/PhysRevD.109.034020

I. INTRODUCTION

The photon provides an important probe to a hadron's internal structure, which historically helped find quantum chromodynamics (QCD) [1,2]. The photon is considered as a clean probe, as its interactions with quarks are primarily through quantum electrodynamics (QED). While this is true for a photon with high virtuality Q^2, the situation gets more complicated at low Q^2. The reason is that, although the photon is an elementary particle, it can quantum fluctuate into other states with the same quantum number in scattering processes, including $\gamma^* \to q\bar{q}$ that contains colored objects. These colored objects interact strongly at low scales and bring nonperturbative QCD effects.

In a light front (or light cone) frame, the splitting amplitudes of $\gamma^* \to q\bar{q}$ are referred to as the photon $q\bar{q}$ light front wave functions (LFWFs) [3–5]. They are interesting by themselves as they encode $q\bar{q}$ components of a photon. Meanwhile, the photon $q\bar{q}$ LFWFs are important input in the color dipole model, which had been applied to the study of various processes such as inclusive and diffractive deep inelastic scattering (DIS) [6–11], diffractive vector meson production [12–15], and ultra-peripheral heavy ion collisions [16–19]. For a few decades, photon LFWFs at leading order QED [3] were employed in color dipole model studies, until next leading order corrections from QCD became available in recent years [20–24]. Meanwhile, the nonperturbative photon LFWFs were also considered in literature [4,25–27]. Therein, a model function was introduced to mimic the nonperturbative effect, with model parameters determined by phenomenological fitting of experiment data. It was found that the inclusion of the nonperturbative QCD corrections in the photon LFWFs improve the description of the experimental data for the observables that are sensitive to color dipoles of large size, namely, with low Q^2 [26,27]. It is also anticipated that the real photons ($Q^2 = 0$) produced in deeply virtual Compton scattering are strongly affected by the nonperturbative effects [25].

On the other hand, to our best knowledge, a theoretical calculation on a photon's nonperturbative $q\bar{q}$ LFWFs at low virtuality is absent in the literature to date. In this paper we will tackle this problem using a light front projection method we introduced in [28]. Therein, a projection formula to extract vector meson $q\bar{q}$ LFWFs from their covariant Bethe-Salpeter (BS) wave functions was given. As the photon is not a composite particle, the meson BS wave functions should be replaced by the photon's inhomogeneous BS wave function, which is essentially the

*cshi@nuaa.edu.cn
†cuibailuo@ahnu.edu.cn
‡wxiangphy@qq.com

covariant (unamputated) quark-photon vertex. The nonperturbative effects in a quark-photon vertex at low Q^2 had long been investigated by the Dyson-Schwinger equations (DSEs) approach [29]. The authors found that by properly dressing the quark-photon vertex, the pion charge radius increases by 50% and gets close to experimental value. Naturally, these nonperturbative effects can be conveyed to photon $q\bar{q}$ LFWFs.

In this paper, we will explore the nonperturbative effects in photon $q\bar{q}$ LFWFs starting with a simplified model, i.e., the contact interaction model within the DSEs. The contact interaction model had been widely employed in the study of various hadron properties [30–39]. Despite the simplicity of the model, it provides a good ground to depict our projection method and calculation techniques. It also renders analytical results on photon $q\bar{q}$ LFWFs, showing intuitively how the nonperturbative effects are encoded in the photon $q\bar{q}$ LFWFs through dressed scalar functions.

This paper is organized as follows. In Sec. II, we introduce the general formalism of photon $q\bar{q}$ LFWFs, as well as the light front projection formula to extract them from covariant quark-photon vertex. In Sec. III, we recapitulate the contact interaction model within the Dyson-Schwinger equations approach and demonstrate the calculation of nonperturbative photon $q\bar{q}$ LFWFs with detail. In Sec. IV, we show that the inclusion of nonperturbative photon LFWFs can improve the agreement between color dipole model calculations and small-x inclusive DIS data at low Q^2. Finally, we summarize in Sec. V.

II. PHOTON $q\bar{q}$ LFWFs

Consider a virtual photon γ^*, including the real photon as the limiting case $Q^2 \to 0$, which schematically has a Fock-state expansion on the light front as

$$|\gamma^*_{\rm phys}\rangle = |\gamma^*_{\rm bare}\rangle + |e^+e^-\rangle_{\gamma^*} + \sum_{f=u,d,s\ldots} |q_f\bar{q}_f\rangle_{\gamma^*} + \ldots. \quad (1)$$

Here the $|e^+e^-\rangle_{\gamma^*}$ can be calculated with perturbative QED. The $|q_f\bar{q}_f\rangle_{\gamma^*}$, on the other hand, is more complicated. At high virtuality, asymptotic freedom allows a perturbative calculation. Yet at low virtuality, the quark and antiquark components interact strongly and the system can be nonperturbative, where nonperturbative QCD method is called for. A general decomposition of $|q_f\bar{q}_f\rangle_{\gamma^*}$ reads

$$|q_f\bar{q}_f\rangle^{\Lambda}_{\gamma^*} = \sum_{\lambda,\lambda';i,j}\int \frac{d^2\boldsymbol{k}_T}{(2\pi)^3}\frac{dx}{2\sqrt{x\bar{x}}}\frac{\delta_{ij}}{\sqrt{3}}\Phi^{\Lambda,(f)}_{\lambda,\lambda'}(x,\boldsymbol{k}_T) \times b^\dagger_{f,\lambda,i}(x,\boldsymbol{k}_T)d^\dagger_{f,\lambda',j}(\bar{x},\bar{\boldsymbol{k}}_T)|0\rangle. \quad (2)$$

The $\Phi^{\Lambda,(f)}_{\lambda,\lambda'}$ is the $q\bar{q}$ LFWF of photon with helicity Λ and quark (antiquark) of flavor $f(\bar{f})$ and spin λ (λ'). The $\Lambda = 0, \pm 1$ and $\lambda = \uparrow$ or $\downarrow$, denoted as $\uparrow = +$ and $\downarrow = -$ for abbreviation in following. The b^+ and d^+ are creation operators of quarks and antiquarks, respectively. The i and j are the color indices. The $\boldsymbol{k}_T = (k^x, k^y)$ is the transverse momentum of the quark, and $\bar{\boldsymbol{k}}_T = -\boldsymbol{k}_T$ for antiquarks.[1] The longitudinal momentum fraction carried by the quark is $x = k^+/P^+$, with $\bar{x} = 1 - x$ for the antiquark. Note that we take the light cone four-vector convention as $A^\pm = \frac{1}{\sqrt{2}}(A^0 \pm A^3)$ and $\boldsymbol{A}_T = (A^1, A^2)$ throughout this paper. Finally, from Eqs. (1) and (2) we can see that the photon $q\bar{q}$ LFWFs are the transition amplitudes of the photon into $q\bar{q}$ states on the light front. They should not be viewed as the light front bound state wave functions, as the photon is not a composite particle.

In [28], we have introduced the light front projection method to obtain $q\bar{q}$ LFWFs of vector mesons from their BS wave functions. The projection formula applies to real and virtual photons as well, e.g.,

$$\Phi^{\Lambda,(f)}_{\lambda,\lambda'}(x,\boldsymbol{k}_T) = -\frac{1}{2\sqrt{3}}\int\frac{dk^-dk^+}{2\pi}\delta(xQ^+ - k^+) \times {\rm Tr}\Big\{\Gamma_{\lambda,\lambda'}\gamma^+ S_f(k)[e_f e\Gamma^{\gamma^*,(f)}(k;Q)\cdot\epsilon_\Lambda(Q)]S_f(k-Q)\Big\}. \quad (3)$$

The $S(k)$ and $\Gamma^{\gamma^*}_\mu(k;Q)$ are the fully dressed quark propagator and (amputated) quark-photon vertex in the momentum space. They can be obtained by solving the quark gap equation and inhomogeneous BS equation, which will be addressed in a later section. The $\epsilon^\mu_\Lambda(Q)$ is the photon polarization vector. The $\Gamma_{\pm,\mp} = I \pm \gamma_5$ and $\Gamma_{\pm,\pm} = \mp(\gamma^1 \mp i\gamma^2)$ project out corresponding quark-antiquark helicity configurations. Note that there is an implicit unit matrix in color space attached to quark propagators and vertices. The trace is taken over Dirac and color indices. We also note that this equation is formulated in Minkowski space. As the contact interaction model we employ takes the Euclidian space, we will transfer our calculation to Euclidian space later, with $q\bar{q}$ LFWFs being the same in two spaces. Finally, we remark that in Eq. (3) we have taken a specific momentum partition, i.e., the momentum of the quark is k and the antiquark is $k - Q$. In a general sense, one can choose $k_\eta = k + \eta Q$ and $k_{\bar{\eta}} = k - (1-\eta)Q$ where η is a real number. In that case, the k^+ in the Dirac δ function in Eq. (3) should be replaced with k^+_η, $S_f(k)$ and $S_f(k-Q)$ should be changed to $S_f(k_\eta)$ and $S_f(k_{\bar{\eta}})$, respectively, and the $q\bar{q}$ LFWFs would remain the same.

Analogous to the case of the vector meson, due to symmetry constraints, the $\Phi^{\Lambda,(f)}_{\lambda,\lambda'}(x,\boldsymbol{k}_T)$'s can generally be expressed with five independent scalar amplitudes $\psi(x,\boldsymbol{k}^2_T)$'s [28,40,41], i.e.,

[1]We take a frame where the virtual photon has no transverse momentum.

$$\Phi^{0,(f)}_{\pm,\mp} = \psi^{0,(f)}_{(1)}, \qquad \Phi^{0,(f)}_{\pm,\pm} = \pm k_T^{(\mp)} \psi^{0,(f)}_{(2)}, \tag{4}$$

$$\Phi^{\pm1,(f)}_{\pm,\pm} = \psi^{1,(f)}_{(1)}, \qquad \Phi^{\pm1,(f)}_{\pm,\mp} = \pm k_T^{(\pm)} \psi^{1,(f)}_{(2)},$$
$$\Phi^{\pm1,(f)}_{\mp,\pm} = \pm k_T^{(\pm)} \psi^{1,(f)}_{(3)}, \qquad \Phi^{\pm1,(f)}_{\mp,\mp} = (k_T^{(\pm)})^2 \psi^{1,(f)}_{(4)}, \tag{5}$$

with $k_T^{(\pm)} = k^x \pm ik^y$, and

$$\psi^{1,(f)}_{(2)}(x, \boldsymbol{k}_T^2) = -\psi^{1,(f)}_{(3)}(1-x, \boldsymbol{k}_T^2). \tag{6}$$

The convention is to take $+$ and $-$ signs in the same row of one equation at once, e.g., $\Phi^{\pm1,(f)}_{\pm,\mp} = \pm k_T^{(\pm)} \psi^{1,(f)}_{(2)}$ means $\Phi^{+1,(f)}_{+,-} = +k_T^{(+)} \psi^{1,(f)}_{(2)}$ and $\Phi^{-1,(f)}_{-,+} = -k_T^{(-)} \psi^{1,(f)}_{(2)}$. In practice, we extract the scalar amplitudes $\psi(x, \boldsymbol{k}_T^2)$'s.

It is convenient to classify the $q\bar{q}$ LFWFs by their quark-antiquark orbital angular momentum projected along the z axis, denoted by l_z. The angular momentum conservation in the z direction then enforces $\Lambda = \lambda + \lambda' + l_z$. Given all possible spin configurations in $\Phi^{\Lambda,(f)}_{\lambda,\lambda'}$, the l_z can be 0, ±1, and ±2, which are s-, p-, and d-wave $q\bar{q}$ LFWFs, respectively. One can also read off the l_z from the power of $k_T^{(\pm)}$ in Eqs. (4) and (5) directly. Note that, in principle, all five amplitudes $\psi(x, \boldsymbol{k}_T^2)$'s are nonzero, yet in a model calculation or at leading order QED, some of them can be vanishing, which will be shown later.

III. THE CONTACT INTERACTION MODEL AND PHOTON LFWFs AT LOW VIRTUALITY

The contact interaction model is a simplified model for strong interaction within the Dyson-Schwinger equations approach. Here we recapitulate the formalism based on [42]. The quark's Dyson-Schwinger equations (or gap equation) formulated in Euclidean space reads

$$S_f(k)^{-1} = i\gamma \cdot k + m_f + \int \frac{d^4q}{(2\pi)^4} g^2 D_{\mu\nu}(k-q) \frac{\lambda^a}{2} \gamma_\mu S_f(q) \frac{\lambda^a}{2} \Gamma_\nu(q;k). \tag{7}$$

In the contact interaction model, one defines

$$g^2 D_{\mu\nu}(k-q) = \delta_{\mu\nu} \frac{4\pi\alpha_{\rm IR}}{m_G^2} \tag{8}$$

with m_G a dynamical mass scale associated with the gluon's infrared behavior.[2] The $\Gamma_\nu(q,k)$ is the Dirac structure part of the quark-gluon vertex. Taking the rainbow truncation, i.e., $\Gamma_\nu(q,k) = \gamma_\mu$, and analogously the ladder approximation for the quark-antiquark interaction kernel, one arrives at the quark gap equation and quark-photon vertex inhomogeneous BS equation,

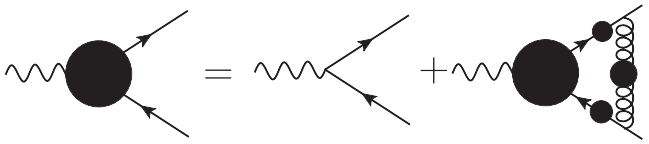

FIG. 1. The diagrammatic representation of inhomogeneous Bethe-Salpeter equation for quark-photon vertex in rainbow-ladder truncation. The black blobs indicate the objects are fully dressed. The dressed gluon propagator here is modeled by contact interaction Eq. (8).

$$S_f^{-1}(k) = i\gamma \cdot k + m_f + \frac{4}{3} \frac{4\pi\alpha_{\rm IR}}{m_G^2} \int \frac{d^4q}{(2\pi)^4} \gamma_\mu S_f(q) \gamma_\mu, \tag{9}$$

$$\Gamma^{\gamma^*,(f)}_\mu(k;Q) = \gamma_\mu - \frac{4}{3} \frac{4\pi\alpha_{\rm IR}}{m_G^2} \int \frac{d^4q}{(2\pi)^4} \times \gamma_\alpha S_f(q) \Gamma^{\gamma^*,(f)}_\mu(q;Q) S_f(q-Q) \gamma_\alpha, \tag{10}$$

Figure 1 displays the Feynman diagram representation for Eq. (10). Intuitively, if perturbation theory is applicable, one can see the $\Gamma^{\gamma^*,(f)}_\mu(k;Q)$ is a sum of infinite diagrams containing ladders of one-gluon exchange at all orders. Yet Eq. (10) is essentially nonperturbative and the $\Gamma^{\gamma^*,(f)}_\mu(k;Q)$ contains all the nonperturbative dynamics. Note that the infinite resummation is also encoded in the fully dressed quark propagator $S_f(k)$ as well.

The solution to Eq. (9) is generally

$$S_f(p)^{-1} = i\gamma \cdot p + M_f, \tag{11}$$

where M_f is a momentum-independent constant. Meanwhile, the contact interaction kernel eliminates the relative momentum k in $\Gamma^{\gamma^*,(f)}_\mu(k;Q)$ and the general form of the solution to Eq. (10) becomes

$$\Gamma^{\gamma^*,(f)}_\mu(Q) = \gamma^T_\mu P^{(f)}_T(Q^2) + \gamma^L_\mu P^{(f)}_L(Q^2), \tag{12}$$

where $\gamma^T_\mu = \gamma_\mu - \frac{Q_\mu \not{Q}}{Q^2}$ and $\gamma^T_\mu + \gamma^L_\mu = \gamma_\mu$. Note that if the k dependence is kept, there will be ten more Dirac structures [29].

In solving Eqs. (9) and (10), proper time regularization is employed. The method is to enforce the replacement

$$\frac{1}{s+M_f^2} = \int_0^\infty d\tau e^{-\tau(s+M_f^2)} \to \int_{\tau_{\rm uv}^2}^{\tau_{\rm ir}^2} d\tau e^{-\tau(s+M_f^2)} \tag{13}$$

[2]This definition takes the notation used in more recent papers such as [35], which makes a simple replacement $\frac{1}{m_G^2} \to \frac{4\pi\alpha_{\rm IR}}{m_G^2}$ in [42].

with $\tau_{\mathrm{ir,uv}}$ infrared and ultraviolet regulators. Finally, the solution to Eqs. (9) and (10) can be summarized as [42]

$$M_f = m_f + \frac{4\alpha_{\mathrm{IR}} M_f}{3\pi m_G^2} \mathcal{C}^{\mathrm{iu}}(M_f^2), \tag{14}$$

$$P_L^{(f)}(Q^2) = 1, \tag{15}$$

$$P_T^{(f)}(Q^2) = \frac{1}{1 + K_\gamma^{(f)}(Q^2)}, \tag{16}$$

with

$$K_\gamma^{(f)}(Q^2) = \frac{4\alpha_{\mathrm{IR}} M_f}{3\pi m_G^2} \int_0^1 d\alpha \alpha(1-\alpha) Q^2 \bar{\mathcal{C}}_1^{iu}(\omega(M_f^2, \alpha, Q^2)), \tag{17}$$

where $\mathcal{C}^{\mathrm{iu}}(M^2)/M^2 = \Gamma(-1, M^2\tau_{\mathrm{uv}}^2) - \Gamma(-1, M^2\tau_{\mathrm{ir}}^2)$, with $\Gamma(\alpha, y)$ being the incomplete Γ function. The notations $\bar{\mathcal{C}}_1^{iu}(z) = \mathcal{C}_1^{iu}(z)/z$, $\mathcal{C}_1^{\mathrm{iu}}(z) = -z(d/dz)\mathcal{C}^{iu}(z)$ and $\omega(M^2, \alpha, P^2) = M^2 + \alpha(1-\alpha)P^2$ are used. The model parameters are set to be $m_G = 0.5$ GeV, $\alpha_{\mathrm{IR}}/\pi = 0.36$, and $\Lambda_{\mathrm{ir}} = 0.24$, $\Lambda_{\mathrm{uv}} = 0.91$, $m_{u/d} = 0.007$, and $m_s = 0.17$ GeV, which well reproduces the meson and baryon spectra [35]. These model parameters yield $M_{u/d} = 0.37$ and $M_s = 0.53$ GeV, so $K_\gamma^{(f)}(Q^2)$ can be determined.

We can now calculate the $q\bar{q}$ LFWFs of the photon through Eq. (3). We first perform a rearrangement of $\Gamma_\mu^{\gamma^*,(f)}(Q)$ in Eq. (12) to be

$$\Gamma_\mu^{\gamma^*,(f)}(Q) = \gamma_\mu P_T^{(f)}(Q^2) + \gamma_\mu^L [P_L^{(f)}(Q^2) - P_T^{(f)}(Q^2)]. \tag{18}$$

In this way, the first term has the Dirac structure of a bare vertex, which is the leading order vertex in QED. Meanwhile, a few notations and relations between four momentums in the Euclidian space are as follows. A four momentum in Euclidian space is $k = (k_1, k_2, k_3, k_4)$, with the first three components corresponding to x, y, and z directions. We separate it into longitudinal and transverse vectors, e.g., $k_\parallel = (\mathbf{0}, k_3, k_4) \equiv (\mathbf{0}, \boldsymbol{k}_\parallel)$ and $k_\perp = (\boldsymbol{k}_\perp, \mathbf{0})$. In Minkowski space, denoting the four-vector of a photon moving in the z direction as $q = (q^0, \mathbf{0}, q^3)$, which satisfies $q^2 = -Q^2$, the polarization vector is taken as $\epsilon_0 = (q^3/Q, \mathbf{0}, q^0/Q)$ [3,43], where the abbreviation $Q \equiv \sqrt{Q^2}$ is used. We introduce a light front null vector $n = 1/\sqrt{2}(1, 0, 0, -1)$, which satisfies $n^2 = 0$ and can be used to project out the plus component of a four-vector, i.e., $n \cdot A = A^+$. Making use of the relation $(A \cdot B)_M \to -(A \cdot B)_E$ from Minkowski to Euclidian space, one can obtain the following useful identities in Euclidian space: $k_\perp \cdot n = 0$, $\epsilon_0 \cdot n = Q \cdot n/Q$, $\epsilon_0 \cdot k_\perp = 0$, and $\epsilon_0 \cdot Q = 0$. Here Q denotes the four momentum of the photon in Euclidian space, and we will use it and $Q = \sqrt{Q^2}$ without distinction, but they can be easily distinguished from the context. Starting with Eqs. (3), (11), and (18), and omitting the flavor index for abbreviation, the derivation goes as

$$\langle x \rangle^m \equiv \int_0^1 dx x^m \Phi^0_{+,-}(x, \boldsymbol{k}_T) \tag{19}$$

$$= -\frac{e_f e P_T(Q^2)}{2\sqrt{3}} \int \frac{d^2\boldsymbol{k}_\parallel}{2\pi} \left(\frac{k^+}{Q^+}\right)^m \frac{1}{|Q^+|} \mathrm{Tr}\left[(I + \gamma^5)\gamma^+ S(k)[\Gamma^{\gamma^*}(k; Q) \cdot \epsilon_0(Q)] S(k - Q)\right] \tag{20}$$

$$= -\frac{e_f e P_T(Q^2)}{2\sqrt{3}|Q \cdot n|} \int \frac{d^2\boldsymbol{k}_\parallel}{2\pi} \left(\frac{k_\parallel \cdot n}{Q \cdot n}\right)^m \frac{\mathrm{Tr}[\not{n}(-i\not{k} + M)\not{\epsilon}_0(-i\not{k} + i\not{Q} + M)]}{(k^2 + M^2)(k^2 - 2k \cdot Q + Q^2 + M^2)} \tag{21}$$

$$= -\frac{\sqrt{N_c} e_f e P_T(Q^2)}{2|Q \cdot n|} \int \frac{d^2\boldsymbol{k}_\parallel}{2\pi} \left(\frac{k_\parallel \cdot n}{Q \cdot n}\right)^m \frac{-2\sqrt{2}[(k_\parallel^2 + k_\perp^2 + M^2 - Q \cdot k_\parallel)(-\sqrt{2}\epsilon_0 \cdot n) + \sqrt{2}(2n \cdot k_\parallel - Q \cdot n)(\epsilon_0 \cdot k_\parallel)]}{(k_\parallel^2 + k_\perp^2 + M^2)(k_\parallel^2 - 2k_\parallel \cdot Q + Q^2 + M^2 + k_\perp^2)} \tag{22}$$

$$= \frac{\sqrt{2N_c} e_f e P_T(Q^2)}{|Q \cdot n|} \int_0^1 du \int \frac{d^2\boldsymbol{k}_\parallel}{2\pi} \left(\frac{k_\parallel \cdot n}{Q \cdot n}\right)^m \frac{(k_\parallel^2 + k_\perp^2 + M^2 - Q \cdot k_\parallel)(-\sqrt{2}\epsilon_0 \cdot n) + \sqrt{2}(2n \cdot k_\parallel - Q \cdot n)(\epsilon_0 \cdot k_\parallel)}{[u(k_\parallel^2 + k_\perp^2 + M^2) + (1-u)(k_\parallel^2 - 2k_\parallel \cdot Q + Q^2 + M^2 + k_\perp^2)]^2} \tag{23}$$

$$= \frac{\sqrt{2N_c} e_f e P_T(Q^2)}{|Q \cdot n|} \int_0^1 du \int \frac{d^2\boldsymbol{k}_\parallel}{2\pi} \left(\frac{k_\parallel \cdot n}{Q \cdot n}\right)^m \frac{(k_\parallel^2 + k_\perp^2 + M^2 - Q \cdot k_\parallel)(-\sqrt{2}\epsilon_0 \cdot n) + \sqrt{2}(2n \cdot k_\parallel - Q \cdot n)(\epsilon_0 \cdot k_\parallel)}{[(k_\parallel - (1-u)Q)^2 + \Delta^2]^2} \tag{24}$$

$$= \frac{\sqrt{2N_c}e_f eP_T(Q^2)}{|Q\cdot n|}\int_0^1 du\int\frac{d^2\boldsymbol{k}_\parallel}{2\pi}\frac{[k_\perp^2+M^2-(1-u)uQ^2](1-u)^m(-\sqrt{2}\epsilon_0\cdot n)}{(k_\parallel^2+\Delta^2)^2} \tag{25}$$

$$= \frac{2\sqrt{N_c}e_f eP_T(Q^2)}{Q}\int_0^1 du'u'^m\int\frac{d^2\boldsymbol{k}_\parallel}{2\pi}\frac{k_\perp^2+M^2-u'(1-u')Q^2}{[k_\parallel^2+Q^2u'(1-u')+M^2+k_\perp^2]^2} \tag{26}$$

$$= \int_0^1 du'u'^m\frac{\sqrt{N_c}e_f eP_T(Q^2)}{Q}\left(1-\frac{2u'(1-u')Q^2}{Q^2u'(1-u')+M^2+k_\perp^2}\right). \tag{27}$$

Comparing Eq. (19) and Eq. (27), we deduce

$$\Phi^0_{+,-}(x,\boldsymbol{k}_T) = e_f eP_T(Q^2)\frac{\sqrt{N_c}}{Q} \times\left(1-\frac{2x(1-x)Q^2}{k_\perp^2+Q^2x(1-x)+M^2}\right). \tag{28}$$

From Eqs. (20) and (21), the trace operation in color space produces an overall color factor N_c and unity in flavor space. The Feynman parametrization technique is implemented in getting Eq. (23). From Eq. (24) to Eq. (25), we have performed a momentum shift in $\boldsymbol{k}_\parallel$. The numerator is fully expanded into polynomials and, due to $n^2=0$, only a few terms survive after integration over $\boldsymbol{k}_\parallel$. We also changed the variable u to $1-u'$ in getting Eq. (26), and the identity

$$\int d^2k\frac{1}{(k^2+A^2)^2} = \frac{\pi}{A^2} \tag{29}$$

is used in getting Eq. (27). Finally, we remark that employing the proper time regularization scheme in calculating the momentum integral in Eq. (26) might be more appropriate from the perspective of an effective model. Yet it would hinder a direct comparison with leading order (LO) QED LFWFs, and since the integral converges, we do not impose the proper time regularization.

Analogously, using Euclidian space relations $\epsilon_{\pm1}\cdot Q=0$, $\epsilon_{\pm1}\cdot n=0$, $\epsilon_{\pm1}\cdot k_\perp = \mp k_T^{(\pm)}$, and $\epsilon_{\pm1}\cdot k_\parallel = 0$ in the photon's collinear reference frame ($\boldsymbol{Q}_\perp=\boldsymbol{0}$), we can derive all other photon $q\bar{q}$ LFWFs, which are summarized as

$$\psi^{0,(f)}_{(1)}(x,\boldsymbol{k}_T^2)\overset{\text{reduced}}{=\!=} -e_f eP_T^{(f)}(Q^2)\frac{\sqrt{N_c}}{Q} \times\frac{2x(1-x)Q^2}{k_\perp^2+Q^2x(1-x)+M_f^2}, \tag{30}$$

$$\psi^{0,(f)}_{(2)}(x,\boldsymbol{k}_T^2) = 0, \tag{31}$$

$$\psi^{1,(f)}_{(1)}(x,\boldsymbol{k}_T^2) = e_f eP_T^{(f)}(Q^2)\sqrt{2N_c}\frac{M_f}{k_\perp^2+Q^2x(1-x)+M_f^2}, \tag{32}$$

$$\psi^{1,(f)}_{(2)}(x,\boldsymbol{k}_T^2) = e_f eP_T^{(f)}(Q^2)\sqrt{2N_c}\frac{x}{k_\perp^2+Q^2x(1-x)+M_f^2}, \tag{33}$$

$$= -\psi^{1,(f)}_{(3)}(1-x,\boldsymbol{k}_T^2), \tag{34}$$

$$\psi^{1,(f)}_{(4)}(x,\boldsymbol{k}_T^2) = 0. \tag{35}$$

Note that, in rewriting Eq. (28) into Eq. (30), we have omitted the unity term, as it becomes a Dirac δ function after Fourier transform with respect to $\boldsymbol{k}_T$ and does not contribute in the color dipole model regarding the cross sections we are interested in.

There are a few remarks worth addressing. Since $\epsilon_\Lambda\cdot Q=0$, which leads to $\epsilon_\Lambda\cdot\gamma_L=0$, the quark-photon vertex in Eq. (18) has only one Dirac structure γ_μ that contributes to Eq. (3). So the quark-photon vertex is equivalent to the bare vertex γ_μ and the quark propagator takes a constituent quark mass M. These are exactly the same structures used in [3] to obtain photon LFWFs, only that therein the light cone perturbation method is employed. In this sense, our derivation confirms that both approaches yield analytically same result. Yet our approach does not rely on the perturbation method and is nonperturbative in essence. In Eqs. (30)–(35), the intrinsic nonperturbative information is encoded in the constituent quark mass M and the quark-photon vertex dressing factor $P_T(Q^2)$.

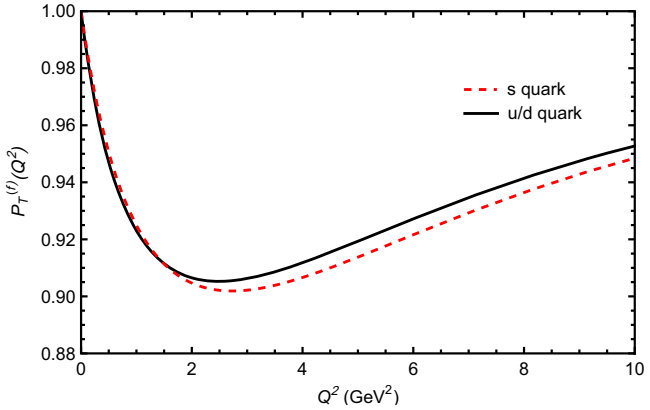

FIG. 2. The $P_T^{(u/d)}(Q^2)$ and $P_T^{(s)}(Q^2)$.

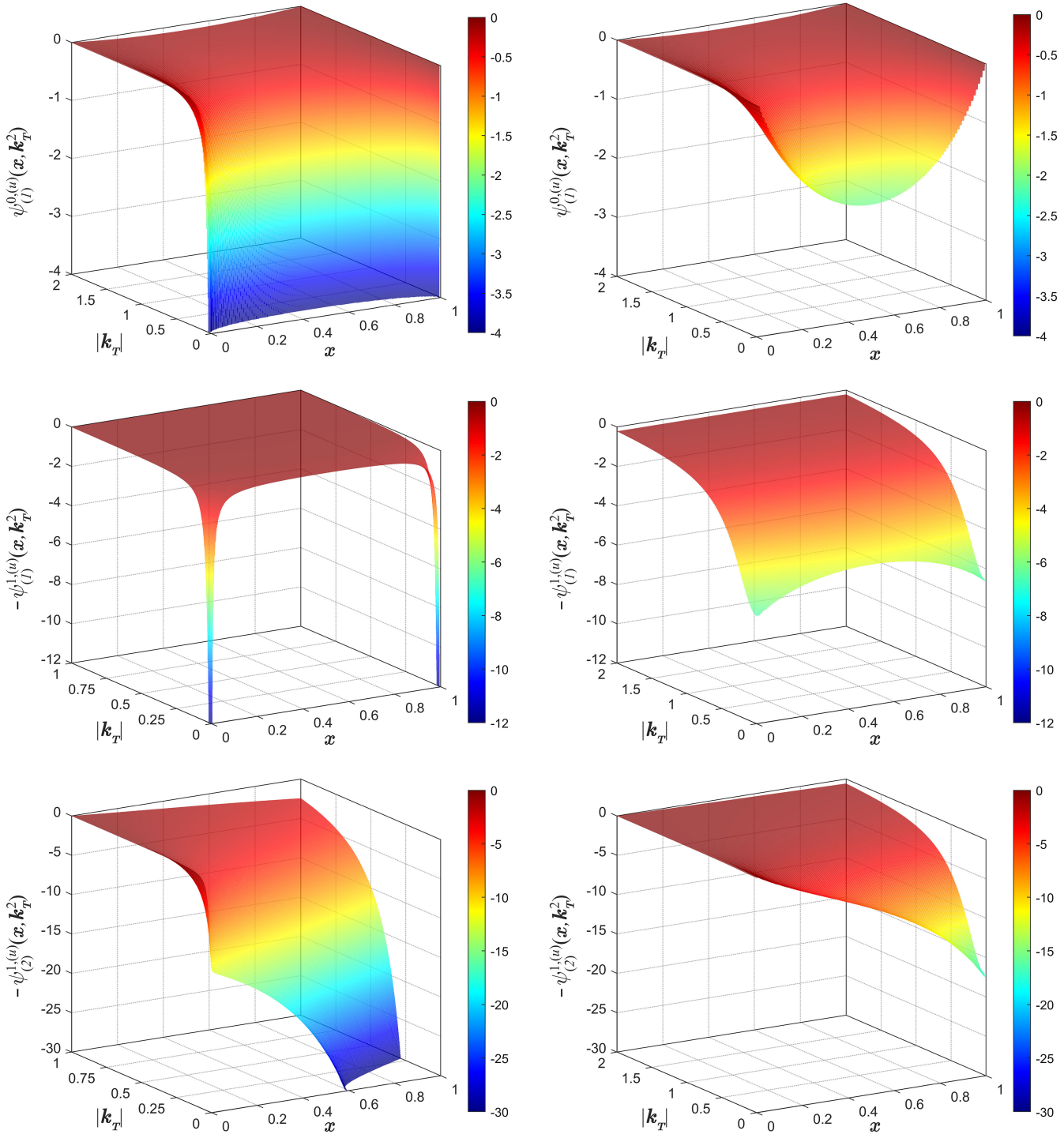

FIG. 3. Photon $u\bar{u}$ LFWFs at a low virtuality $Q^2 = 0.2$ GeV^2. The perturbative LFWFs are shown in the left column and nonperturbative ones are in the right column. See Eq. (5) for definition of the $\psi(x, \boldsymbol{k}_T^2)$'s.

We remind the reader that the $M_{u/d/s}$ is generally 2 orders of magnitude larger than the current quark mass. It is a direct reflection of the chiral symmetry breaking in QCD, as well as the nonperturbative dynamics. In this connection, a quark mass around 140 MeV that was popular in the color glass condensate (CGC) model fitting to the HERA data [44] seems to be a compromise between constituent quark mass around 300–400 MeV and partonlike current quark mass. In addition, we also notice a multiplicative (and nonperturbative) factor $P_T(Q^2)$ in Eq. (28). It brings a few percents of suppression to photon $q\bar{q}$ LFWFs at low Q^2, as shown in Fig. 2, but reduces to unity at $Q^2 = 0$. In Fig. 3 we show the 3D plot of perturbative and nonperturbative photon $q\bar{q}$ LFWFs at $Q^2 = 0.2$ GeV^2

for comparison. The perturbative photon $u\bar{u}$ LFWFs are in the left column. They are strongly peaked at low $|\boldsymbol{k}_T|$ so a small portion of the surface extends beyond the plots. On the other hand, taking nonperturbative effects into account, the peaks get suppressed and the LFWFs change significantly.

The limitations in our result should also be kept in mind. First, due to the contact interaction model, the quark-photon vertex has only one Dirac structure γ_μ that contributes. If one employs a more realistic model that allows $\Gamma^{\gamma^*}_\mu(k;Q)$ to be dependent on k, ten more Dirac structures would appear, such as $k_\mu, k_\mu \not{Q}$, etc. In that case, the $\psi^0_{(2)}$ and $\psi^1_{(4)}$ will no longer be vanishing, i.e., p- and d-wave components could appear. Such property has been observed in the study of vector meson leading Fock-state LFWFs [28]. Second, the contact interaction model works at low energy so our result [Eqs. (30)–(35)] only holds for low Q^2. At large Q^2, the photon LFWFs should approach the perturbative result. Therefore, we expect a complete photon LFWF from low to high Q^2 should undergo a transition from our nonperturbative LFWFs to the perturbative ones.

IV. INCORPORATING NONPERTURBATIVE PHOTON $q\bar{q}$ LFWFs IN SMALL-x DIS

The inclusive ep DIS at small x can be described by the color dipole model [6,7,45], in which a virtual photon is emitted by the incoming electron and then splits into a color dipole that scatters with proton inelastically. The cross section takes the factorized form

$$\sigma^{\gamma^* p}_{L,T}(x,Q^2) = 2\sum_f \int d^2\boldsymbol{r} \int d^2\boldsymbol{b} \int_0^1 dz |\Psi^{(f)}_{L,T}(z,r;Q^2)|^2 \times \mathcal{N}(x^{(f)},r,b), \tag{36}$$

where

$$|\Psi^{(f)}_T(r,z;Q^2)|^2 = \frac{1}{2}\sum_{\lambda,\bar{\lambda}'}\Big[|\tilde{\Phi}^{1,(f)}_{\lambda,\bar{\lambda}'}(r,z;Q^2)|^2 + \tilde{\Phi}^{-1,(f)}_{\lambda,\bar{\lambda}'}(r,z;Q^2)|^2\Big], \tag{37}$$

$$|\Psi^{(f)}_L(r,z;Q^2)|^2 = \sum_{\lambda,\bar{\lambda}'}|\tilde{\Phi}^{0,(f)}_{\lambda,\bar{\lambda}'}(r,z;Q^2)|^2 \tag{38}$$

are the squared photon $q\bar{q}$ LFWFs. The $\tilde{\Phi}$ is defined as the photon $q\bar{q}$ LFWFs in coordinate space, e.g.,

$$\tilde{\Phi}^{\Lambda,(f)}_{\lambda,\lambda'}(z,\boldsymbol{r}) = \int \frac{d^2\boldsymbol{k}}{(2\pi)^2} e^{i\boldsymbol{k}\cdot\boldsymbol{r}} \Phi^{\Lambda,(f)}_{\lambda,\lambda'}(z,\boldsymbol{k}). \tag{39}$$

In this work we take the light quarks (u, d, and s) and charm quark into account. In this case the $x^{(f)}$ equals Bjorken-x for light quarks, and $x^{(c)} = x(1+4m_c^2/Q^2)$ for the charm quark.

The $\mathcal{N}(x,r,b)$ is the imaginary part of the forward dipole-proton scattering amplitude, with color dipole transverse size r and collision impact parameter b. Here we employ the bCGC model [44,46], which reads

$$\mathcal{N}(x,r,b) = \begin{cases} N_0\left(\frac{rQ_s}{2}\right)^{2\gamma_{\rm eff}} & rQ_s \le 2, \\ 1-\exp[-\mathcal{A}\ln^2(\mathcal{B}rQ_s)] & rQ_s > 2, \end{cases} \tag{40}$$

with

$$Q_s(x,b) = \left(\frac{x_0}{x}\right)^{\frac{\lambda}{2}} \exp\left[-\frac{b^2}{4\gamma_s B_{\rm CGC}}\right], \tag{41}$$

$$\gamma_{\rm eff} = \gamma_s + \frac{1}{\kappa\lambda Y}\ln\left(\frac{2}{rQ_s}\right), \tag{42}$$

$$Y = \ln(1/x), \tag{43}$$

and

$$\mathcal{A} = -\frac{N_0^2\gamma_s^2}{(1-N_0)^2\ln(1-N_0)}, \tag{44}$$

$$\mathcal{B} = \frac{1}{2}(1-N_0)^{-\frac{1-N_0}{N_0\gamma_s}}. \tag{45}$$

The $\kappa = 9.9$ is fixed to be the LO Balitsky-Fadin-Kuraev-Lipatov value, and $B_{\rm CGC} = 5.5\ {\rm GeV}^{-2}$ determined by fitting exclusive meson production data in [46]. Other model parameters N_0, γ_s, x_0, and λ are determined by fitting inclusive DIS data [46]. In this work, we employ the reduced cross section σ_r data from HERA [47], which is a linear combination of proton structure functions F_2 and F_L, i.e.,

$$\sigma_r(x,y,Q^2) = F_2(x,Q^2) - \frac{y^2}{1+(1-y)^2}F_L(x,Q^2) \tag{46}$$

with

$$F_2(x,Q^2) = \frac{Q^2}{4\pi^2\alpha_{\rm em}}[\sigma_L^{\gamma^* p}(x,Q^2) + \sigma_T^{\gamma^* p}(x,Q^2)], \tag{47}$$

$$F_L(x,Q^2) = \frac{Q^2}{4\pi^2\alpha_{\rm em}}\sigma_L^{\gamma^* p}(x,Q^2). \tag{48}$$

The $y = Q^2/(sx)$ is the inelasticity parameter and s is the center of mass energy square.

From Eq. (36) we can see the inclusive DIS cross section is the convolution between the square of LFWFs and the color dipole model. This makes the $\sigma_r(x,y,Q^2)$ sensitive to photon LFWFs. From high to low Q^2, the color dipole gets larger in size and the nonperturbative effect should emerge. We can therefore investigate whether the nonperturbative photon $q\bar{q}$ LFWFs can play a role at low Q^2.

TABLE I. Fitting the reduced DIS cross section data of HERA [47] with the *b*CGC model using nonperturbative-effect modified photon LFWFs [Eq. (49)]. The current quark masses are set to physical values $m_{u/d} = 4$ MeV, $m_s = 95$ MeV, and $m_c = 1.27$ GeV. The dressed quark mass $M_{u/d/s}$ and dressing function $P_T^{(u/d/s)}(Q^2)$ are determined by the contact interaction model in Sec. III.

LFWFs [Eqs. (30)–(35), (49)]	Q^2/GeV^2	γ_s	N_0	x_0	λ	Q_0^2	n	$\chi^2/\mathrm{d.o.f.}$
Perturbative	[0.85, 50]	0.6290	0.4199	2.395×10^{-4}	0.1962	⋯	⋯	$265.8/223 = 1.192$
Perturbative	[0.25, 50]	0.3869	0.7556	7.047×10^{-7}	0.1052	⋯	⋯	$678.4/282 = 2.406$
Perturbative + Nonperturbative	[0.25, 50]	0.6177	0.4596	1.326×10^{-4}	0.1875	1.052	3.970	$337.9/280 = 1.207$

As perturbative photon $q\bar{q}$ LFWFs are applicable at large Q^2, and our nonperturbative photon $q\bar{q}$ LFWFs only work at low Q^2, we introduce a modified model that linearly combines the two, i.e.,

$$|\Psi'^{(f)}_{T,L}(r,z;Q^2)|^2 = F_{\mathrm{part}}(Q^2)|\Psi^{(f),\mathrm{np}}_{T,L}(r,z;Q^2)|^2 + [1 - F_{\mathrm{part}}(Q^2)]|\Psi^{(f),\mathrm{p}}_{T,L}(r,z;Q^2)|^2 \tag{49}$$

with a Q^2-dependent weighting factor

$$F_{\mathrm{part}}(Q^2) = \frac{Q_0^{2n}}{(Q^2 + Q_0^2)^n}. \tag{50}$$

We remind the reader that the nonperturbative $\Psi^{(f),\mathrm{np}}_{T,L}$ uses Eqs. (30)–(35), and the perturbative term $\Psi^{(f),\mathrm{p}}_{T,L}$ can be obtained by setting $P_T(Q^2) = 1$ and $M_f = m_f$ in Eqs. (30)–(35). The two parameters Q_0 and n modulate the rising of the nonperturbative effect. We further assume the Q_0 and n are the same for u/d and s quarks. For the heavy charm quark, we ignore the nonperturbative effect for now, as it is supposed to be small due to the large intrinsic scale brought by quark mass. A quantitative check will be left for future investigation. At large Q^2, $F_{\mathrm{part}}(Q^2)$ approaches zero so the $|\Psi'^{(f)}_{T,L}(r,z;Q^2)|^2$ is dominated by perturbative photon $q\bar{q}$ LFWFs $|\Psi^{(f),\mathrm{p}}_{T,L}(r,z;Q^2)|^2$. As Q^2 decreases, $F_{\mathrm{part}}(Q^2)$ increases and $|\Psi'^{(f)}_{T,L}(r,z;Q^2)|^2$ starts to pick up contributions from nonperturbative photon LFWFs $|\Psi^{(f),\mathrm{np}}_{T,L}(r,z;Q^2)|^2$, until the LFWFs become completely nonperturbative at $Q^2 = 0$ GeV^2.

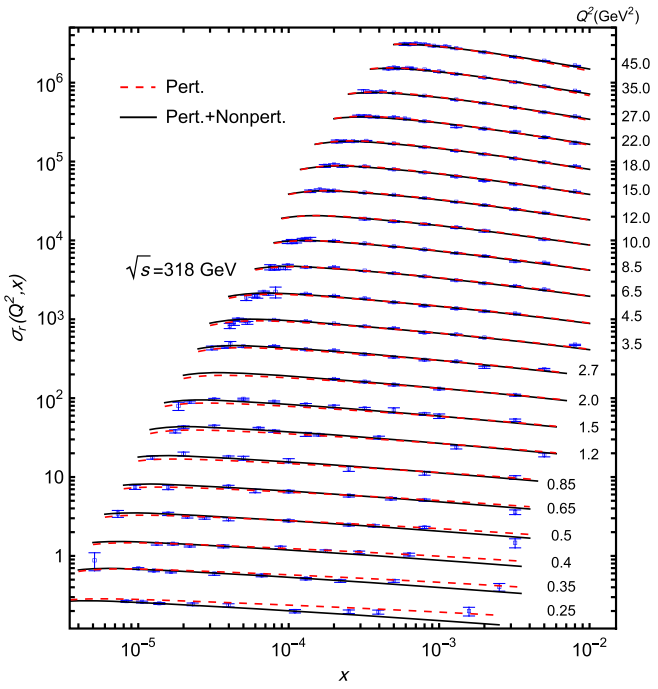

FIG. 4. The reduced cross section σ_r of DIS at $\sqrt{s} = 318$ GeV. Data points are taken from [47] and curves are calculated using parameters from the third (black solid) and second (red dashed) rows of Table I.

We then fit the reduced cross section data [47] with $|\Psi'^{(f)}_{T,L}(r,z;Q^2)|^2$. The employed data are limited to $x < 0.01$ and $Q^2 < 50$ GeV^2. We remind the reader that in [46] the authors found that, when current quark masses are employed in perturbative photon LFWFs, the *b*CGC model can well fit HERA data only for $Q^2 \geq 0.85$ GeV^2. This is reasonable, as the photon LFWFs can only approach the perturbative form for certain large Q^2. Here with nonperturbative corrections, our result is shown in Table I. The first column indicates whether perturbative- (LO QED and QCD) or the nonperturbative-effect modified photon LFWFs are employed. The first row shows that data of $Q^2 \in [0.85, 50]$ GeV^2 can be fitted using perturbative photon LFWFs with current quark masses, in agreement with [46]. Here the determined parameters are a bit different from those in [46] as we use $m_{u/d} = 4$ and $m_s = 95$ MeV, while therein $m_s = m_{u/d} \approx 0$ MeV. To investigate nonperturbative effects, we then employ data to lower Q^2, e.g., $Q^2 \approx \Lambda^2_{\mathrm{QCD}}$. We find that, for $Q^2 \in [0.25, 50]$ GeV^2, the fitting with perturbative photon LFWFs (second row) becomes significantly worse, while that incorporating nonperturbative effects (third row) remains good.[3] Figures 4 and 5 show the HERA σ_r data as compared to calculated cross section using parameters in

[3]Note that, to accommodate low Q^2 data, the *b*CGC model parameters in the third row are quite different from those in the first row. However, if the model parameters in row one are used, we will get $\chi^2 \approx 2000$ for data of $Q^2 \in [0.25, 50]$ GeV^2, which is unreasonable.

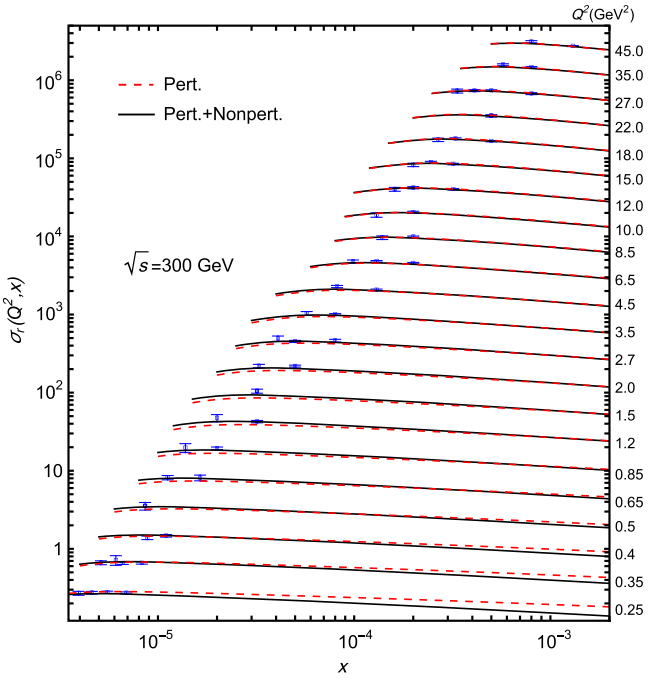

FIG. 5. The reduced cross section σ_r of DIS at $\sqrt{s} = 300$ GeV. Data points are taken from [47] and curves are calculated using parameters from the third (black solid) and second (red dashed) rows of Table I.

the second (red dashed) and third (black solid) rows of Table I. Since $F_{\text{part}}(Q^2)$ is a positive definite function, this result strongly suggests that incorporating the nonperturbative photon $q\bar{q}$ LFWFs can significantly improve the agreement between color dipole model calculations and inclusive small-x DIS data at low Q^2.

V. SUMMARY

Circumventing the light front quantization procedure, the photon $q\bar{q}$ LFWFs can be extracted from covariant the unamputated quark-photon vertex, which is available from various nonperturbative QCD methods or models that are quantized in ordinary space-time. In this paper, we resort to a contact interaction model. With this particular model, the nonperturbative effects are encoded in the enhanced quark mass M and a dressing factor $P_T(Q^2)$ that both arise through nonperturbative dynamics, as compared to LO QED photon LFWFs. In particular, for a real photon $P_T(Q^2 = 0) = 1$, so the nonperturbative effects are totally absorbed into the enhanced quark mass M. The QCD's dynamical chiral symmetry breaking property thus plays a significant role in shaping the photon $q\bar{q}$ LFWFs at low Q^2.

Within the color dipole model, the cross section of inclusive DIS is an integral of the squared photon $q\bar{q}$ LFWFs, and hence is sensitive to photon LFWFs. We then modify the perturbative photon LFWFs by incorporating nonperturbative effects at low Q^2 through Eq. (49). It is found that this modification can significantly improve the agreement between the color dipole model and small-x inclusive DIS HERA data toward the lower Q^2 region, in agreement with earlier works using a phenomenological model [4,25–27].

Finally, we remind the reader that, in the present work, the nonperturbative photon LFWFs in Eqs. (30)–(35) are limited to some unknown low Q^2. They do not transform into perturbative ones at large Q^2 by themselves. The transition is thus modeled by a primitive function (50). Yet this limitation is not brought by the projection method [Eq. (3)], but is rooted in the contact interaction model, which only works at low scales. It can be overcame by employing a covariant unamputated quark-photon vertex that contains both infrared and ultraviolet dynamics. In this connection, the Maris-Tandy model within the Dyson-Schwinger equations approach [48,49], along with other studies of the quark-photon vertex formulated in ordinary space-time, can be considered as good candidates for future study.

ACKNOWLEDGMENTS

C. S. is grateful for Ya-Ping Xie and Pei-Lin Yin for helpful suggestions. This work was supported by the Fundamental Research Funds for the Central Universities (under Grant No. 1227050553), the National Natural Science Foundation of China (under Grants No. 11905104 and No. 12165004), the Education Department of Guizhou Province under Grant No. QJJ[2022]016, the Strategic Priority Research Program of Chinese Academy of Sciences (under Grant No. XDB34030301), and Nanjing Overseas Scholars Innovation Project Selective Financial Support.

[1] M. Breidenbach, J. I. Friedman, H. W. Kendall, E. D. Bloom, D. H. Coward, H. C. DeStaebler, J. Drees, L. W. Mo, and R. E. Taylor, Phys. Rev. Lett. **23**, 935 (1969).
[2] E. D. Bloom *et al.*, Phys. Rev. Lett. **23**, 930 (1969).
[3] H. G. Dosch, T. Gousset, G. Kulzinger, and H. J. Pirner, Phys. Rev. D **55**, 2602 (1997).
[4] J. R. Forshaw, R. Sandapen, and G. Shaw, Phys. Rev. D **69**, 094013 (2004).

[5] T. Lappi, H. Mäntysaari, and J. Penttala, Phys. Rev. D **102**, 054020 (2020).
[6] N. N. Nikolaev and B. G. Zakharov, Z. Phys. C **49**, 607 (1991).
[7] H. Kowalski and D. Teaney, Phys. Rev. D **68**, 114005 (2003).
[8] C. Marquet, Phys. Rev. D **76**, 094017 (2007).
[9] A. H. Rezaeian, M. Siddikov, M. Van de Klundert, and R. Venugopalan, Phys. Rev. D **87**, 034002 (2013).
[10] H. Mäntysaari and B. Schenke, Phys. Rev. Lett. **117**, 052301 (2016).
[11] H. Mäntysaari and P. Zurita, Phys. Rev. D **98**, 036002 (2018).
[12] H. Kowalski, L. Motyka, and G. Watt, Phys. Rev. D **74**, 074016 (2006).
[13] J. R. Forshaw and R. Sandapen, Phys. Rev. Lett. **109**, 081601 (2012).
[14] A. Arroyo Garcia, M. Hentschinski, and K. Kutak, Phys. Lett. B **795**, 569 (2019).
[15] M. Li, Y. Li, G. Chen, T. Lappi, and J. P. Vary, Eur. Phys. J. C **82**, 1045 (2022).
[16] V. P. Goncalves and M. V. T. Machado, Eur. Phys. J. C **40**, 519 (2005).
[17] T. Lappi and H. Mantysaari, Phys. Rev. C **87**, 032201 (2013).
[18] Y.-p. Xie and X. Chen, Eur. Phys. J. C **76**, 316 (2016).
[19] V. P. Gonçalves, M. V. T. Machado, B. D. Moreira, F. S. Navarra, and G. S. dos Santos, Phys. Rev. D **96**, 094027 (2017).
[20] G. Beuf, Phys. Rev. D **94**, 054016 (2016).
[21] G. Beuf, T. Lappi, and R. Paatelainen, Phys. Rev. D **104**, 056032 (2021).
[22] G. Beuf, T. Lappi, and R. Paatelainen, Phys. Rev. D **106**, 034013 (2022).
[23] G. Beuf, H. Hänninen, T. Lappi, Y. Mulian, and H. Mäntysaari, Phys. Rev. D **106**, 094014 (2022).
[24] G. Beuf, T. Lappi, and R. Paatelainen, Phys. Rev. Lett. **129**, 072001 (2022).
[25] C. Flensburg, G. Gustafson, and L. Lonnblad, Eur. Phys. J. C **60**, 233 (2009).
[26] J. Berger and A. M. Stasto, J. High Energy Phys. 01 (2013) 001.
[27] V. P. Gonçalves and B. D. Moreira, Eur. Phys. J. C **80**, 492 (2020).
[28] C. Shi, Y.-P. Xie, M. Li, X. Chen, and H.-S. Zong, Phys. Rev. D **104**, L091902 (2021).
[29] P. Maris and P. C. Tandy, Phys. Rev. C **61**, 045202 (2000).
[30] L. X. Gutierrez-Guerrero, A. Bashir, I. C. Cloet, and C. D. Roberts, Phys. Rev. C **81**, 065202 (2010).
[31] C. Chen, L. Chang, C. D. Roberts, S. M. Schmidt, S. Wan, and D. J. Wilson, Phys. Rev. C **87**, 045207 (2013).
[32] S.-S. Xu, C. Chen, I. C. Cloet, C. D. Roberts, J. Segovia, and H.-S. Zong, Phys. Rev. D **92**, 114034 (2015).
[33] M. A. Bedolla, J. J. Cobos-Martínez, and A. Bashir, Phys. Rev. D **92**, 054031 (2015).
[34] F. E. Serna, B. El-Bennich, and G. a. Krein, Phys. Rev. D **96**, 014013 (2017).
[35] P.-L. Yin, C. Chen, G. a. Krein, C. D. Roberts, J. Segovia, and S.-S. Xu, Phys. Rev. D **100**, 034008 (2019).
[36] P.-L. Yin, Z.-F. Cui, C. D. Roberts, and J. Segovia, Eur. Phys. J. C **81**, 327 (2021).
[37] X. Wang, Z. Xing, J. Kang, K. Raya, and L. Chang, Phys. Rev. D **106**, 054016 (2022).
[38] Z. Xing and L. Chang, Phys. Rev. D **107**, 014019 (2023).
[39] B. A. Zamora, E. C. Martínez, J. Segovia, and J. J. Cobos-Martínez, Phys. Rev. D **107**, 114031 (2023).
[40] J. Carbonell, B. Desplanques, V. A. Karmanov, and J. F. Mathiot, Phys. Rep. **300**, 215 (1998).
[41] X.-d. Ji, J.-P. Ma, and F. Yuan, Phys. Rev. Lett. **90**, 241601 (2003).
[42] H. L. L. Roberts, C. D. Roberts, A. Bashir, L. X. Gutierrez-Guerrero, and P. C. Tandy, Phys. Rev. C **82**, 065202 (2010).
[43] Y. V. Kovchegov and E. Levin, *Quantum Chromodynamics at High Energy* (Oxford University Press, New York, 2013), Vol. 33, 10.1017/9781009291446.
[44] G. Watt and H. Kowalski, Phys. Rev. D **78**, 014016 (2008).
[45] A. H. Mueller, Nucl. Phys. **B415**, 373 (1994).
[46] A. H. Rezaeian and I. Schmidt, Phys. Rev. D **88**, 074016 (2013).
[47] H. Abramowicz *et al.* (H1 and ZEUS Collaborations), Eur. Phys. J. C **75**, 580 (2015).
[48] P. Maris and C. D. Roberts, Phys. Rev. C **56**, 3369 (1997).
[49] P. Maris and P. C. Tandy, Phys. Rev. C **60**, 055214 (1999).